IEEE Access
Multidisciplinary | Rapid Review | Open Access Journal

Received 7 February 2024, accepted 29 February 2024, date of publication 5 March 2024, date of current version 14 March 2024.

Digital Object Identifier 10.1109/ACCESS.2024.3373869

RESEARCH ARTICLE

Dual Bandwidth Enhancement Using a New Multi-Resonance Feeding Structure for 5G Communication

RUI LI[1], LONGYUE QU[2,3], (Member, IEEE), SEOK-JU WI[1], HUANXUAN REN[4], AND HYEONGDONG KIM[1]

[1]Department of Electronic Engineering, Hanyang University, Seoul 04763, South Korea
[2]Department of Electronics and Information Engineering, Harbin Institute of Technology, Shenzhen 518055, China
[3]Guangdong Provincial Key Laboratory of Aerospace Communication and Networking Technology, Harbin Institute of Technology, Shenzhen 518055, China
[4]Department of Automation, Shandong University of Science and Technology, Jinan 250100, China

Corresponding author: Hyeongdong Kim (hdkim@hanyang.ac.kr)

This work was supported by the Natural Research Foundation of Korea through a grant from Korean Government (Ministry of Science and ICT) under Grant 2019R1F1A1063993.

ABSTRACT This paper introduces a multi-resonance feed structure to control the input impedance for achieving a dual wide-impedance bandwidth technology. According to the simulation, the bandwidth of the proposed antenna structure was approximately 330 MHz with the lower band (ranging from 670 MHz to 1000 MHz) and 1210 MHz with the higher band (ranging from 1670 MHz to 2880 MHz) under a 3:1 voltage standing wave ratio. Moreover, the average efficiency was significantly increased from 26.6% (reference) to 46.5% (proposed) at the lower band (ranging from 550 MHz to 1020 MHz) and even higher at the higher band, increasing from 15.5% (reference) to 61.2% (proposed) (ranging from 1400 MHz to 3000 MHz). The radiation pattern also showed satisfactory antenna radiation performance. This proposed technology has the advantage of achieving input impedance matching more easily and covers most fifth-generation (5G) NR operating bands in FR1 (n1, n3, n5, n8, n25, n30, n41, n66), indicating its promising application to 5G communication.

INDEX TERMS Impedance matching, wideband, coupling, 5G communication, antenna feeds.

I. INTRODUCTION

Over the past several years, the increased penetration of mobile communication into more aspects of life has greatly changed people's lives and communication abilities. The convenience of 4G technology has already solved the problem of communication anytime and anywhere [1]. At the same time, with the rapid development of the mobile Internet, new businesses and services continue to be produced, and mobile data traffic is also growing rapidly. It may be difficult for 4G communication systems to meet the increasing demand for mobile data traffic [2]. To address both concerns, the development of the fifth-generation (5G) mobile communication technology has become a focus for many researchers [3], [4], [5], [6], [7]. In particular, the sub-6GHz antenna design has been popularly studied for mobile devices to solve the target of diffraction ability and coverage effect for sub-6 GHz; there are more and more requirements for 5G communication wide band technology [8], [9], [10], [11], [12], [13], [14], [15]. In the meantime, the demand for the miniaturization of mobile devices is also increasing, which means area constraints for the antenna continue to rise. However, the antenna performance and bandwidth decrease as the antenna's physical area shrinks [16], [17]. As a result, over the past several decades, the development of high-efficiency, wide-bandwidth, and miniature antennas has played an important role in mobile device communication development [18], [19], [20].

In previous studies investigating wide-bandwidth technologies, the methods of increasing the dual impedance bandwidth can be approximately divided into two approaches. The most common way is to use the multi-resonance antenna

The associate editor coordinating the review of this manuscript and approving it for publication was Bilal Khawaja.

feed structure for exciting the antenna to achieve multiband operation [21], [22]. Enhanced dual-band impedance bandwidth can be realized using a series-resonance feed structure with two series resonators [23]. In [24], [25], and [26], these studies are mainly applied to the efficiency of multi-resonance antenna feed structures. This kind of method is mainly used to control the input impedance matching of the antenna by adjusting the ratio of inductance and capacitance in the feed structure to realize the wideband technology. Another class of methods uses other structures; for example, a dual-band branch-line coupler structure has been proposed with operating frequencies of 0.9 GHz to 2.0 GHz [27]. Controlling the characteristic mode of the metal rim can also enhance the antenna bandwidth and performance [28], [29]. Additionally, a micro-strip feed monopole antenna design method can achieve wideband performance [30]. In addition, antenna design using the characteristic mode of the printed circuit board (PCB) can also realize wideband antenna technology [31], [32], [33], [34], [35], [36], [37]. These approaches have been influential in the field of wideband antenna design recently. However, they often occupy excessive physical space on the PCB or impose specific requirements for the physical location of the antenna design, making it difficult to achieve the goal of antenna miniaturization. Consequently, this paper focuses on improving the multi-resonance antenna feed structure method to establish a novel multi-resonance feed structure and control the input impedance of the dual-impedance bandwidth more conveniently and distinctly.

In this paper, we used the multi-resonance feeding structure to control the antenna input impedance to achieve the dual wide impedance bandwidth technology for 5G communication applications. We used the proposed multi-resonance feeding structure with a series capacitor to control the coupling performance with the lower and higher dual bands. Here, a parallel capacitor mainly controlled the resonance frequency of the lower band, and a shunt capacitor controlled the resonance frequency of the higher band to achieve the proposed antenna input impedance matching. The proposed antenna was designed in the PCB and achieved the bandwidth at a low frequency of 330 MHz (ranging from 670 MHz to 1000 MHz) and a high frequency of 1210 MHz (ranging from 1670 MHz to 2880 MHz) under a 3:1 voltage standing wave ratio. The measurement results also showed satisfactory performance with a bandwidth of 354 MHz (ranging from 664 MHz to 1018 MHz) in the lower band and a bandwidth of 1490 MHz (ranging from 1390 MHz to 2880 MHz) in the higher band under a 3:1 voltage standing wave ratio. Additionally, the average efficiency increased from 26.6% (reference) to 46.5% (proposed) in the lower band at 670 MHz to 1020 MHz and from 15.5% (reference) to 61.2% (proposed) in the higher band at 1400 MHz to 3000 MHz. This covers the target frequency bands of 5G NR FR1, where most operating bands have frequencies of 690–960 MHz (n5, n8, n12) or 1690–2690 MHz (n1, n3, n7, n30, n34, n41). The proposed antenna has a wider bandwidth and better efficiency compared to antennas operating in the same frequency bands as those in previous studies. It also allows for easier manipulation of the impedance matching. It is worth noting that the proposed technology can be applied to different scenarios including different evaluation board sizes, materials, and feeding structure sizes. This proposed technology has strong prospects in the development of 5G communication applications.

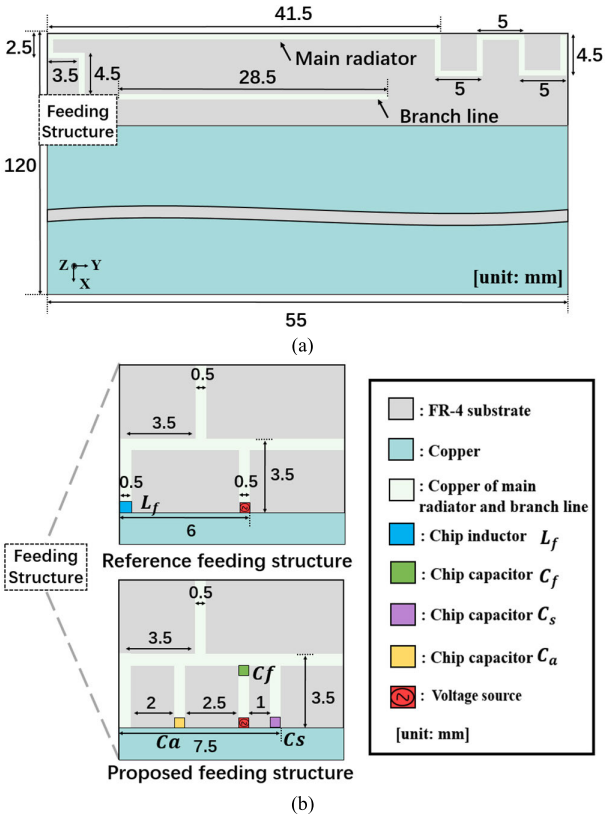

FIGURE 1. Geometries of the (a) reference and proposed ground planes. (b) The feeding structure of the reference and the proposed antenna.

II. ANTENNA DESIGN

The geometries of the reference antenna and proposed antenna are set on a 120 mm × 55 mm × 1 mm PCB on a frame retardant type 4 (FR-4) substrate ($\varepsilon_r = 4.4, \boldsymbol{tan}\delta = 0.02$) as shown in Figure 1. The size of the ground plane is 110 mm × 55 mm with a clearance of 10 mm × 55 mm at the top of the board used for the antenna design. The width of the main radiator and branch line in this simulation operation is set to 0.5 mm. The antenna comprises a proposed feeding structure that determines input impedance matching, an antenna element (simple quarter-wavelength type), and a branch line that determines the antenna's lower band and higher band resonance frequency. The reference antenna feeding structure with a size of 3.5 mm × 6.0 mm and a series with a chip inductor $\boldsymbol{L_f}$ (4 nH) with only one loop current, i.e., the same as the planar inverted-F antenna (PIFA), were used to achieve the reference antenna input impedance matching. The proposed antenna

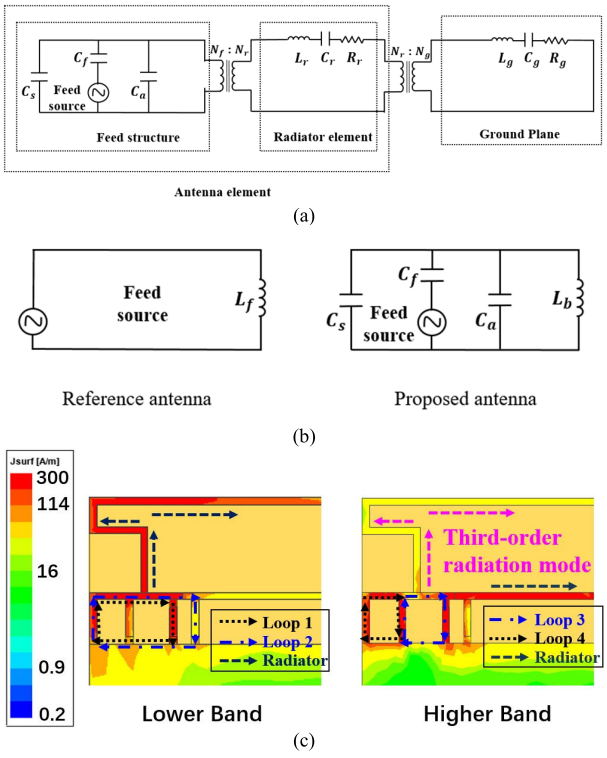

FIGURE 2. (a) Diagrammatic sketch of the proposed antenna structure, resonance loop (radiator element including the main radiator and branch line), and ground plane. (b) Simplified reference and proposed antenna feeding structures. (c) Simulated surface current distributions with the proposed antenna.

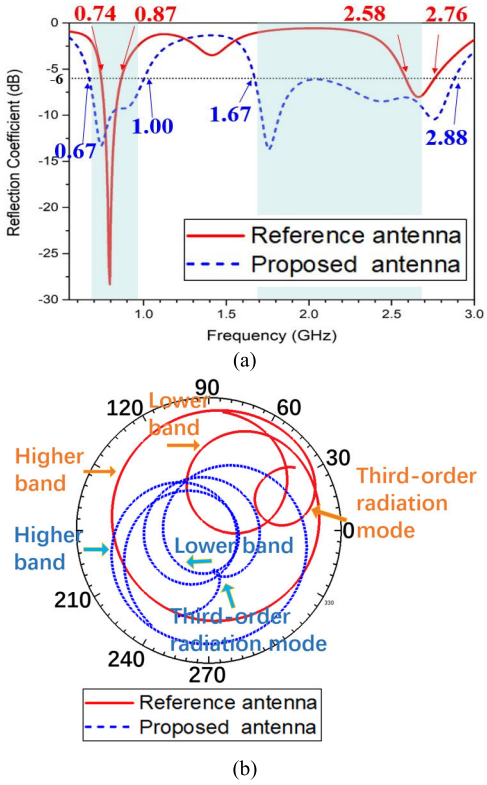

FIGURE 3. Simulated results of the reference and proposed antennas. (a) Reflection coefficient, and (b) Input impedance loci in the Smith chart.

used a 3.5 mm × 7.5 mm feed structure. The feeding point with a series chip capacitor $\boldsymbol{C_f}$ (4.2 pF), shunt chip capacitors $\boldsymbol{C_a}$ (1.9 pF), and parallel chip capacitor $\boldsymbol{C_s}$ (0.8 pF) were used for the proposed antenna input impedance matching. The reference and proposed antennas were designed and analyzed using the simulation software Ansys HFSS. Notably, the proposed technology can be applied to different scenarios, including evaluation board sizes, materials, and feeding structure sizes.

Figure 2. (a) shows the diagrammatic sketch circuit model of the antenna elements and ground plane as an equivalent series RLC circuit composed of R_g, L_g, and C_g. Figure 2. (b) shows the simplified reference and proposed antenna feeding structures; it can be seen that the proposed antenna feeding structure has more circuit loops than the reference antenna feeding structure. The lower band impedance matching between Loop 1 and Loop 2 in the two-port impedance [Z] matrix can be expressed as [16], [38], and [42]:

$$[\mathrm{Z}] = \begin{bmatrix} j\left(\omega L_{Loop1} - \frac{1}{\omega C_f}\right) & j\omega L_{Loop1} \\ j\omega L_{Loop1} & j\left(\omega L_{Loop2} - \frac{1}{\omega C_s}\right) \end{bmatrix} \quad (1)$$

Loop 1 consists of the shorting pin, the series chip capacitor (C_f), the parallel chip capacitor (C_s), and the feeding point. Loop 2 is composed of the shorting pin, and the parallel chip capacitor (C_s). Loop 1, Loop 2, and the main radiator set that achieves the antenna lower band wideband operating technology. The impedance matching using Z_{11}, Z_{12}, and Z_{22} between Loop 3 and Loop 4 with the higher band in the two-port impedance can be expressed as [42]:

$$\begin{aligned} \mathrm{Z}_{in} &= \mathrm{Z}_{11} - \frac{Z_{12}^2}{Z_{22}} \\ &= j\left(\omega L_{Loop3} - \frac{1}{\omega(C_a)}\right) - \frac{(\omega L_{C_f})^2}{j\left(\omega L_{Loop4} - \frac{1}{\omega(C_f + C_a)}\right)} \end{aligned} \quad (2)$$

in Eqs. (1) and (2), components L_{loopn} are the inductances of Loop1-4 in the feeding structure, where L_{C_f} is the impedance of the shorting series capacitor (C_f) line. The Loop 3 current consists of the shorting pin and the chip capacitor (C_a), and the Loop 4 current consists of the series capacitor (C_f) and the chip capacitor (C_a). Figure 2. (c) shows the surface current distributions with the proposed antenna of the lower and higher bands. (Including the third-order radiation mode.) During the feeding structure operation of the proposed antenna, it can be seen that multiple Loop 3, Loop 4, branch line, and the main radiator (third-order radiation mode) are set as the antenna's higher band operating frequency, achieving the wide impedance bandwidth.

III. SIMULATION RESULTS AND OPERATION PRINCIPLE

The simulation results with the reference and proposed antennas are shown in Figure 3. The reflection coefficient using the reference antenna was a −6 dB bandwidth

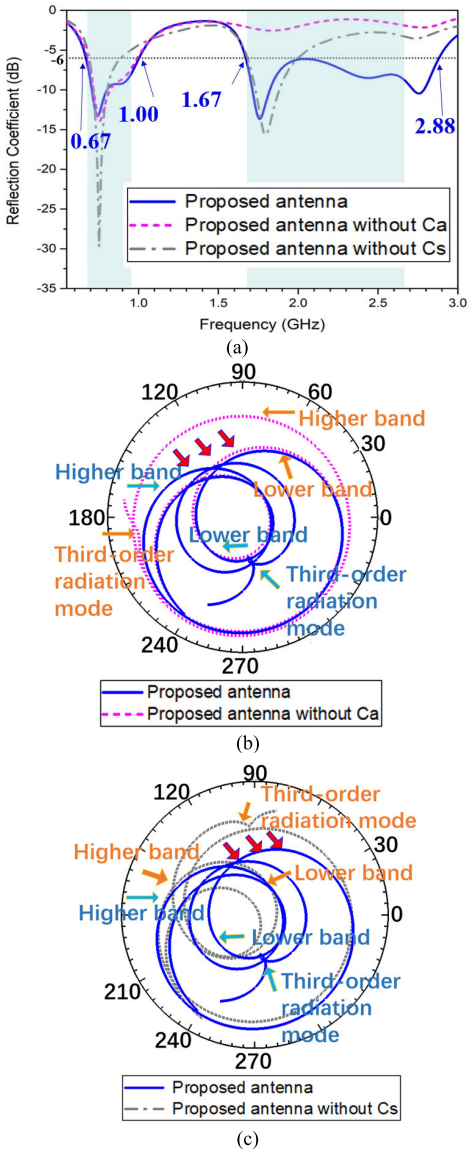

FIGURE 4. Simulated results. (a) Reflection coefficient, and Input impedance loci in a Smith chart (b) without chip capacitor C_a, (c) chip capacitor C_s.

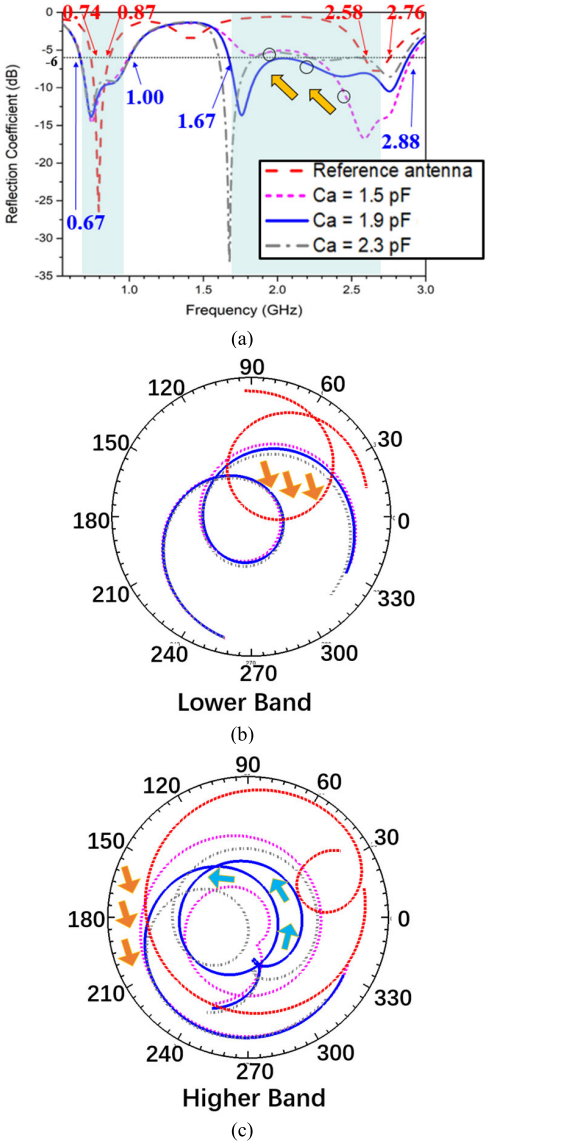

FIGURE 5. Simulated results of the reference and proposed antennas with different shunt chip capacitors C_a. (a) Reflection coefficient. Input impedance loci in a Smith chart of (b) the lower and (c) the higher bands.

of 130 MHz (ranging from 0.74 GHz to 0.87 GHz) with the lower band and a −6 dB bandwidth of 180 MHz (ranging from 2.58 GHz to 2.76 GHz) with the higher band, as shown in Figure 3. The proposed antenna achieved a −6 dB bandwidth of 330 MHz (ranging from 0.67 GHz to 1.00 GHz) with the lower band and a −6 dB bandwidth of 1210 MHz (ranging from 1.67 GHz to 2.88 GHz) with the higher band, which fully covers the 5G NR target operating band (from 0.69 GHz to 0.96 GHz and 1.69 GHz to 2.69 GHz). The −6 dB bandwidth corresponding to a VSWR of 3 is generally used, even though a VSWR of 2 is also used in some cases [7], [15], [20]. Figure 3. (b) shows the input impedance loci in a Smith chart with the reference and proposed antennas. Compared with the reference antenna, the normalized input impedance of the proposed antenna was closer to the 50 Ω point. (The third-order radiation mode is the higher-order mode of the main radiator.)

To better understand the antenna operating principle, Figure 4. (a) shows the simulated reflection coefficients of the proposed antenna and the proposed antenna without a chip capacitor (C_a or C_s). To match the input impedance for the situation without chip capacitor C_a, the value of the parallel chip capacitor (C_s) is converted to 1.2 pF to achieve lower band impedance bandwidth matching. As depicted in Figure 4. (a), a −6 dB bandwidth of 310 MHz (ranging from 0.68 GHz to 0.99 GHz) in the situation without chip capacitor C_a shows a similar performance to the proposed antenna for the lower band. It can be observed that the reflection coefficient of the higher band part has improved significantly with the shunt chip capacitor C_a added, which proved the

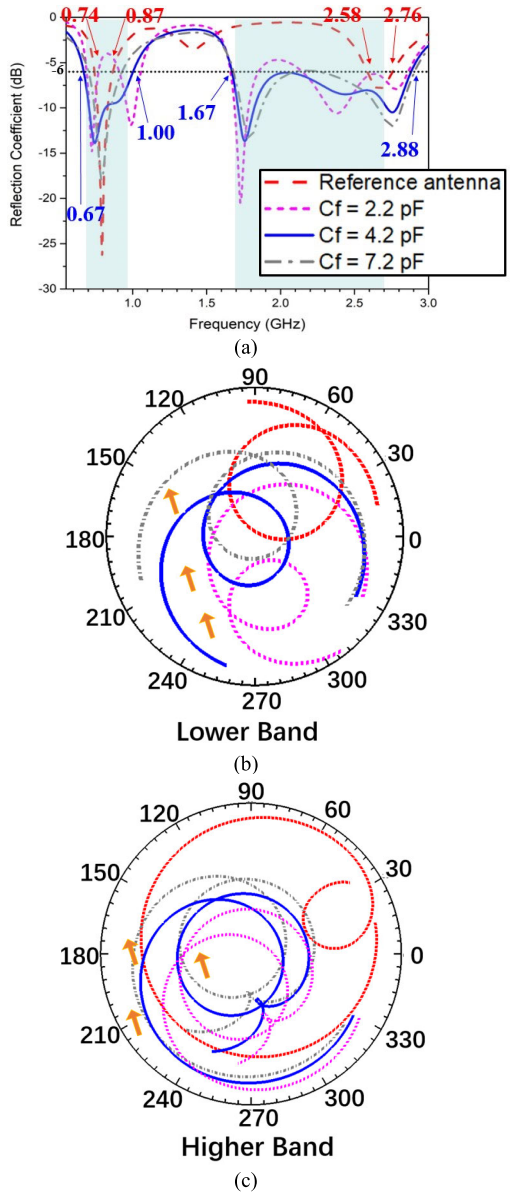

FIGURE 6. Simulated results of the reference and proposed antennas with different series chip capacitors C_f. (a) Reflection coefficient. Input impedance loci in a Smith chart of (b) the lower and (c) the higher bands.

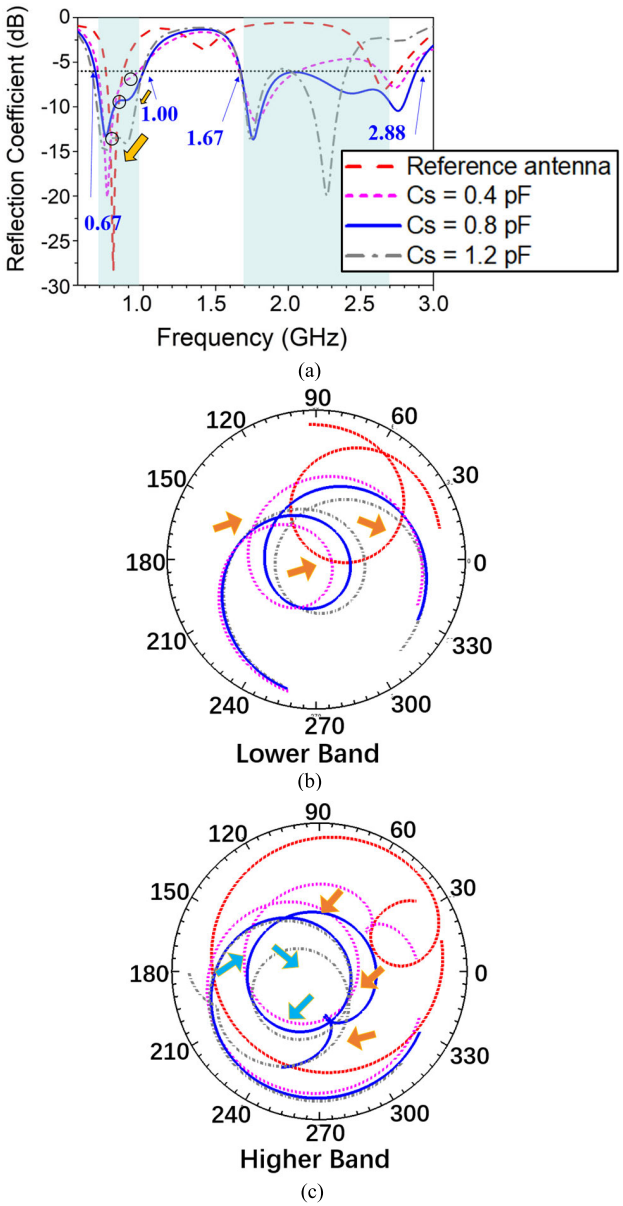

FIGURE 7. Simulated results of the reference and proposed antenna with different parallel chip capacitors C_s. (a) Reflection coefficient. Input impedance loci in a Smith chart of (b) the lower and (c) the higher bands.

chip capacitor C_a is the main factor controlling the input impedance of the higher band.

The series capacitor (C_f) and the parallel capacitor (C_s) controlled the input impedance matching for the lower band. When the new shunt chip capacitor (C_a) was added, the higher-band loci moved from the outside to the inside of the -6 dB circle for the normalized input impedance loci in the Smith chart, closer to the 50 Ω point (as shown in Figure 4. (b)). After adding the shunt chip capacitor (C_a), series chip capacitor (C_f), and parallel chip capacitor (C_s) to the reference antenna, the proposed antenna current mode differed from the reference antenna (one-loop current) due to the multi-resonance feeding structure, achieving a lower and higher wideband technology. Therefore, the added shunt chip capacitor (C_a) controls the higher band input impedance.

Figure 5. (a) shows simulated reflection coefficients of the reference and proposed antennas with different shunt chip capacitor (ca) values ranging from 1.5 pF to 2.3 pF. It can be observed that the resonance frequency of the lower band is not changed significantly, and the higher band frequency decreased with the increase of the shunt chip capacitor (C_a) values. For the input impedance loci with an increase in the shunt chip capacitor (C_a) value, the path of the input impedance loci circle moved slightly outward (coupling increased gradually) in the lower band at 0.55 GHz to 1.2 GHz. However, this was not due decisively to the

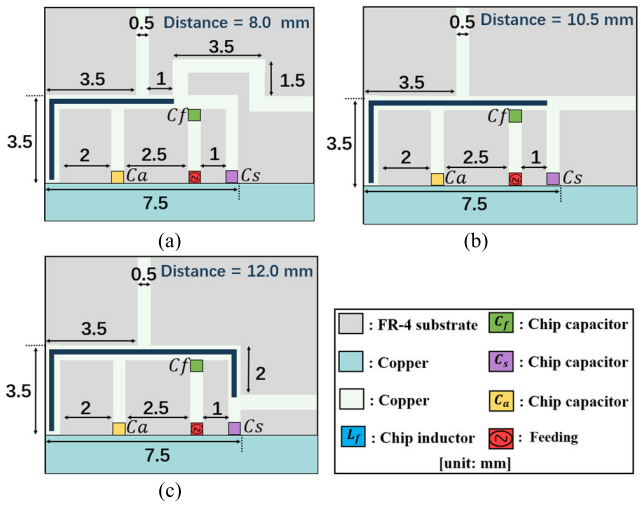

FIGURE 8. Geometry of the proposed antenna branch line with different contact distance values. (a) Distance = 8.0 mm. (b) Distance = 10.5 mm. (c) Distance = 12.0 mm.

coupling performance with the lower band, as shown in Figure 5. (b). In the higher band at 1.2 GHz to 3.0 GHz, as shown in Figure 5. (c), the input impedance loci extended outward with increasing shunt chip capacitor (C_a) values (coupling and resonance frequency decreased), and the path of the small locus circle rotated in the counter-clockwise direction. Figure 6. (a) depicts the reflection coefficients of the reference and the proposed antennas with different series chip capacitor (C_f) values ranging from 2.2 pF to 7.2 pF. By observing the reflection coefficient, the lower band and higher band frequencies were not changed significantly with the increase of the series chip capacitor (C_f) values. The series chip capacitors (C_f) controlled the coupling performance of the lower bands, as shown in Figure 6. (b), such that the path of the input impedance loci circle moved outward (coupling increased) in the lower band at 0.55 GHz to 1.2 GHz. In the higher band at 1.2 GHz to 3.0 GHz, as shown in Figure 6. (c), the input impedance loci circle extended outward (coupling increases), and the resonance frequency was also reduced.

Figure 7. (a) shows the simulated reflection coefficients of the reference and proposed antennas with different parallel chip capacitor (C_s) values ranging from 1.5 pF to 2.3 pF. It can be observed that the resonance frequency of the lower band has decreased slightly with the increase of the parallel chip capacitor (C_s) values. For the lower band input impedance loci circle at 0.55 GHz to 1.2 GHz, as shown in Figure 7. (b), the resonance frequency decreases with an increased parallel chip capacitor (C_s) value such that the loci circle moved slightly inward (the coupling decreased gradually). The path of the small locus circle rotated clockwise. Figure 7. (c) shows the input impedance loci circle at 1.2 GHz to 3.0 GHz; when the parallel chip capacitor (C_s) value increased, the loci circle moved inward gradually (not decisive with coupling performance), and the small-locus circle with the higher band also rotated clockwise.

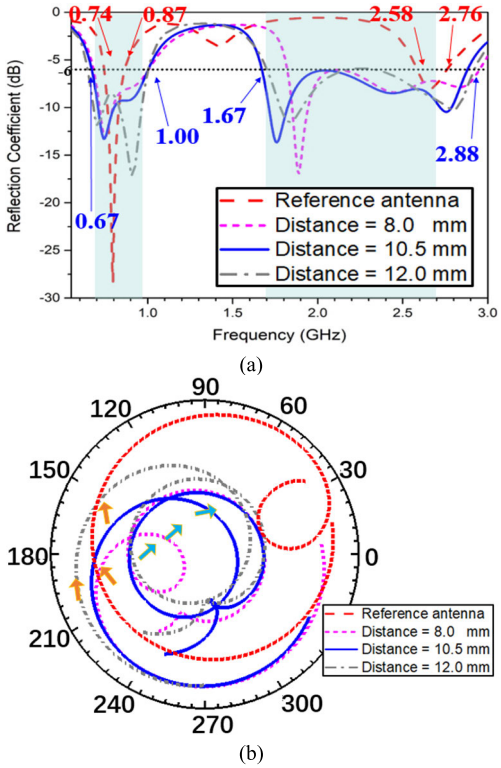

FIGURE 9. Simulated reflection coefficients of the reference and proposed antenna with different distance values. (a) Reflection coefficient (b) Input impedance loci in the Smith Chart (1.2 GHz to 3.0 GHz).

To better explore the control method of the higher band small locus circle, the proposed antenna branch line contact point moves on the proposed antenna feeding structure at different distances with the dark blue line from 8.0 mm to 12.0 mm, as shown in Figure 8. Figure 9. (a) shows the simulated reflection coefficients with the different contact distance values; it can be seen that when the distance increased, the size of the small locus circle became larger and rotated clockwise in the higher band at 1.2 GHz to 3.0 GHz (as shown in Figure 9. (b)). As a result, the series capacitor (C_f) controls the size of the lower band and higher band input impedance locus (coupling size). The parallel capacitor (C_s) mainly controls the resonance frequency of the lower band. The shunt capacitor (C_a) mainly controls the resonance frequency of the higher band, while the size of the lower band's small locus circle is determined by the contact distance from the antenna element to the feeding structure. The size of the higher band's small locus circle is determined by the contact distance from the branch line to the feeding structure.

IV. EXPERIMENTAL RESULTS

The reference and the proposed antennas were fabricated and measured using Agilent 8753ES network analyzers and a 6 m × 3 m × 3 m 3D CITA OTA chamber as shown in Figure 10. (a). The series chip inductor L_f (4 nH) was used with the measurement reference antenna structure. The reference antenna covers a −6 dB bandwidth of 140 MHz (ranging from 730 MHz to 870 MHz) in

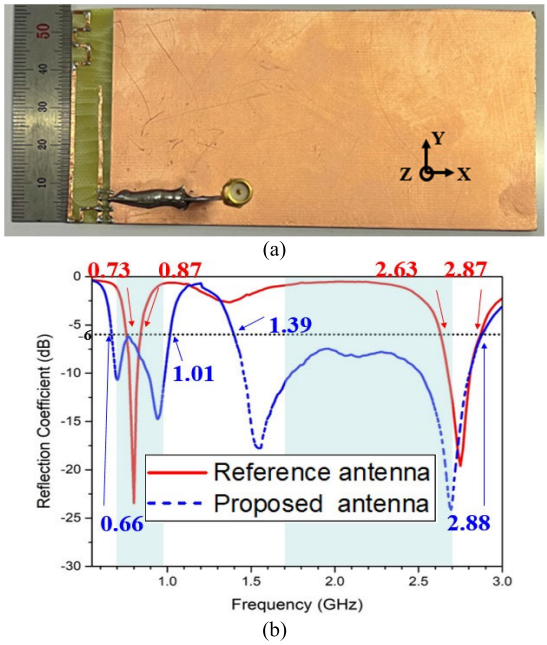

FIGURE 10. (a) Fabricated the proposed antenna prototype. (b) Measured reflection coefficients of the reference and proposed antenna.

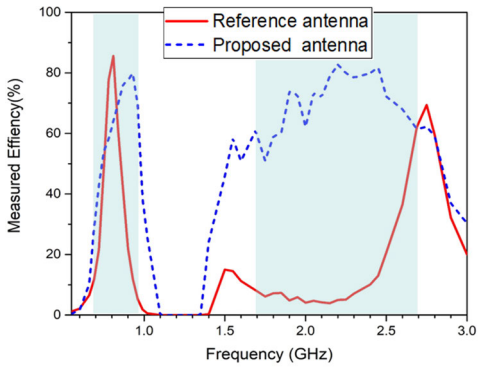

FIGURE 11. Measured efficiency of the reference and proposed antenna.

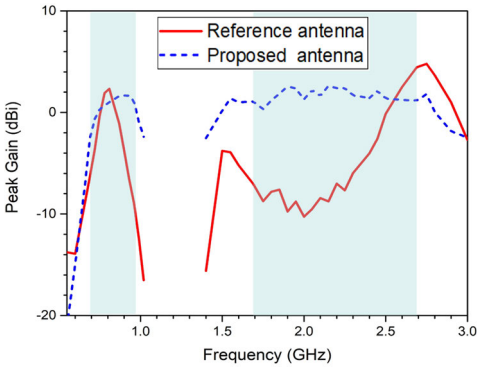

FIGURE 12. Measured Peak Gain of the reference and proposed antenna.

the lower band and a −6 dB bandwidth of 240 MHz (ranging from 2630 MHz to 2870 MHz) in the higher band. In the proposed antenna structure, the series chip capacitor C_f is 4.0 pF, the parallel chip capacitor C_s is 0.5 pF, and the shunt chip capacitor C_a is 2.2 pF to

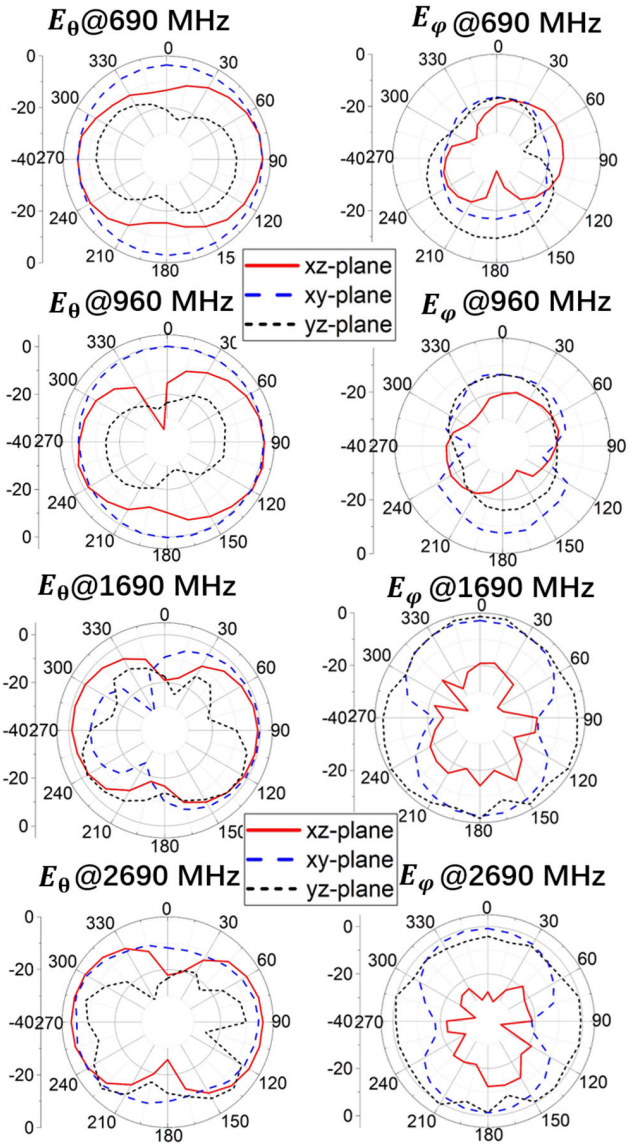

FIGURE 13. Measured far-field omnidirectional radiation patterns of the proposed antenna with E_θ and E_φ, at 690 MHz, 960 MHz, 1690 MHz, and 2690 MHz.

achieve input impedance matching. The −6 dB bandwidth of 354 MHz (ranging from 664 MHz to 1018 MHz) increased by 214 MHz in the lower band. Additionally, the bandwidth of 1490 MHz (ranging from 1390 MHz to 2880 MHz) increased by 1250 MHz in the higher band to cover the target frequency bands (690–960 MHz to 1690–2690 MHz), as shown in Figure 10. (b).

The measurement results show similar performance to the simulation results, and the proposed antenna achieves a wide bandwidth using the proposed technology. Figure 11. shows the measured efficiency of the reference and proposed antennas. For the lower band (550–1020 MHz), the reference antenna's average measured efficiency is 26.6%, while the proposed antenna's is 46.5%, an increase of 19.9%. For the higher band (1400-3000 MHz), the efficiency of the reference antenna is 15.5% and the efficiency of the proposed antenna

TABLE 1. Comparison results of the proposed antenna with those in the reference literature.

Study	Overall Size(mm)	BW (MHz)	Antenna Efficiency	Operating Frequency (GHz)	Antenna Type
[20]	110 × 50 × 5	241(-6dB)	58.5%	0.73 – 0.974	PIFA
[21]	110 × 55 × 0.5	309/1116(-6dB)	53.5%/57.8%	0.694 – 1.003/1.656 – 2.772	PIFA
[39]	60 × 115 × 1	520/610(-6dB)	33.45%/45.71%	0.7 – 1.4/1.7 – 2.2	IFA
[40]	70 × 140 × 1	420(-6dB)	51%	3.4 – 3.6	IFA
[41]	40 × 45 × 1.0	1700/1600(-10dB)	76.5%/69.5%/61.7%	2.3 – 4.1/5.0 – 6.6	Monopole
Proposed	120 × 55 × 1	330/1210(-6dB)	46.5%/61.2%	0.67 – 1.0/1.67 – 2.88	PIFA

is 61.2%, which is an increase of 45.7%. The measured proposed antenna peak gain obtained is 1.66 dB at 900 MHz, and 2.62 dB at 2150 MHz as shown in Figure 12. Figure 13. shows the measured radiation patterns of the proposed antenna at target frequencies of 690 MHz, 960 MHz, 1690 MHz, and 2690 MHz, with good omnidirectional performance. The measurement results show that the antenna bandwidth was improved by using the proposed technology. Table 1 compares the results of the proposed antenna with previous studies in terms of the PCB size, bandwidth, antenna efficiency, operating frequency band, and antenna type [20], [21], [39], [40], [41]. It can be observed that the proposed antenna has a wider bandwidth and better efficiency compared with antennas of the same type in the same operating frequency bands. The proposed antenna also allows for easier manipulation of the impedance matching compared with previous studies.

V. CONCLUSION

In this paper, we propose a multi-resonance feeding structure with a series capacitor to control the coupling performance with lower and higher dual bands. The parallel capacitor mainly controls the resonance frequency of the lower band and the shunt capacitor controls the resonance frequency of the higher band, achieving input impedance matching with the proposed antenna. In a simulation under a 3:1 voltage standing wave ratio, the proposed antenna achieved a bandwidth of 330 MHz in the lower band (ranging from 670 MHz to 1000 MHz) and 1210 MHz in the higher band (ranging from 1670 MHz to 2880 MHz). Additionally, the average efficiency increased from 26.6% (reference) to 46.5% (proposed) in the lower band at 670 MHz to 1020 MHz and from 15.5% (reference) to 61.2% (proposed) in the higher band from 1400 MHz to 3000 MHz, achieving the intended target frequency bands of most 5G NR FR1 bands (n5, n8, n12) with a frequency of 690–960 MHz and (n1, n3, n7, n30, n34, n41) with a frequency of 1690–2690 MHz. Therefore, this technology has potential in 5G communication applications.

ACKNOWLEDGMENT

(Rui Li and Longyue Qu contributed equally to this work.)

REFERENCES

[1] A. Sibille, C. Oestges, and A. Zanella, *MIMO: From Theory to Implementation*. San Diego, CA, USA: Academic Press, 2011.
[2] F. Boccardi, R. W. Heath, A. Lozano, T. L. Marzetta, and P. Popovski, "Five disruptive technology directions for 5G," *IEEE Commun. Mag.*, vol. 52, no. 2, pp. 74–80, Feb. 2014.
[3] T. D. Nguyen, Y. Lee, and C. W. Jung, "Transparent and flexible patch antenna using MMF for conformal WiFi-6E applications," *J. Electromagn. Eng. Sci.*, vol. 23, no. 4, pp. 310–317, Jul. 2023.
[4] X. Liu, S. Gao, B. Sanz-Izquierdo, H. Zhang, L. Wen, W. Hu, Q. Luo, J. T. S. Sumantyo, and X.-X. Yang, "A mutual-coupling-suppressed dual-band dual-polarized base station antenna using multiple folded-dipole antenna," *IEEE Trans. Antennas Propag.*, vol. 70, no. 12, pp. 11582–11594, Dec. 2022.
[5] J. Xu, X. Xia, K.-M. Luk, and W. Hong, "Millimeter-wave array antennas using broadband 3D folded strip elements for B5G/6G communications," *IEEE Trans. Antennas Propag.*, vol. 70, no. 12, pp. 11569–11581, Dec. 2022.
[6] J. Yin, Y. Jia, S. Yang, and H. Zhai, "Design of a composite decoupling structure for dual-band dual-polarized base station array," *IEEE Antennas Wireless Propag. Lett.*, vol. 21, pp. 1408–1412, 2022.
[7] L. A. Iliadis, V. P. Rekkas, A. D. Boursianis, P. Sarigiannidis, G. K. Karagiannidis, C. Christodoulou, and S. K. Goudos, "Triple-band modified printed inverted-F antenna design for Wi-Fi-7 applications," in *Proc. 17th Eur. Conf. Antennas Propag. (EuCAP)*, Mar. 2023, pp. 1–4.
[8] Y. Liu, S. Wang, N. Li, J.-B. Wang, and J. Zhao, "A compact dual-band dual-polarized antenna with filtering structures for sub-6 GHz base station applications," *IEEE Antennas Wireless Propag. Lett.*, vol. 17, pp. 1764–1768, 2018.
[9] Z. Duan, S. Shen, and G. Wen, "A compact tri-band filtering antenna system for 5G sub-6 GHz applications," *IEEE Trans. Antennas Propag.*, vol. 70, no. 11, pp. 11097–11102, Nov. 2022.
[10] R. Hussain, "Shared-aperture slot-based sub-6-GHz and mm-wave IoT antenna for 5G applications," *IEEE Internet Things J.*, vol. 8, no. 13, pp. 10807–10814, Jul. 2021.
[11] L. Sang, B. Hu, J. Wang, F. Dong, and Q. Chen, "An UWB 3-D rolled-up delay line for phased array systems in the 5G sub-6 GHz frequency band," *IEEE Microw. Wireless Compon. Lett.*, vol. 32, no. 9, pp. 1119–1122, Sep. 2022.
[12] Q. Liang, H. Aliakbari, and B. K. Lau, "Co-designed millimeter-wave and sub-6 GHz antenna for 5G smartphones," *IEEE Antennas Wireless Propag. Lett.*, vol. 21, pp. 1995–1999, 2022.
[13] Y. Shi and W. Wang, "A transparent wideband dual-polarized antenna for sub-6 Ghz application," *IEEE Trans. Antennas Propag. Lett.*, vol. 21, no. 10, pp. 2020–2024, Oct. 2022.
[14] Z. Zahid and L. Qu, "Colocated MIMO antenna pair based on modal orthogonality for 5G terminal applications," *Microw. Opt. Technol. Lett.*, vol. 64, no. 11, pp. 2044–2051, Nov. 2022.
[15] Y. Jeon and B. Kim, "Design of a 0.5–18 GHz wideband frequency down-converter module with a local circuit for an electronic support measurement system," *J. Electromagn. Eng. Sci.*, vol. 22, no. 2, pp. 103–113, Mar. 2022.
[16] Z. Zahid and H. Kim, "Coupling mechanism of a loop-type ground radiation antenna," *ETRI J.*, vol. 41, no. 4, pp. 528–535, Aug. 2019.
[17] S. Jeon and H. Kim, "Mobile terminal antenna using a planar inverted-e feed structure for enhanced impedance bandwidth," *Microw. Opt. Technol. Lett.*, vol. 54, no. 9, pp. 2133–2139, Sep. 2012.
[18] O. Cho, H. Choi, and H. Kim, "Loop-type ground antenna using a capacitor," *Electron. Lett.*, vol. 41, no. 1, pp. 11–12, Jan. 2011.
[19] Y. Liu, X. Lu, H. Jang, H. Choi, K. Jung, and H. Kim, "Loop-type ground antenna using resonated loop feeding, intended for mobile devices," *Electron. Lett.*, vol. 47, no. 7, pp. 426–427, 2011.

[20] J. Lee, Y. Liu, H. H. Kim, and H. Kim, "PIFA with dual-resonance feed structure for enhancement of impedance bandwidth," *Electron. Lett.*, vol. 49, no. 15, pp. 921–922, Jul. 2013.
[21] J. Lee, Y. Liu, and H. Kim, "Mobile antenna using multi-resonance feed structure for wideband operation," *IEEE Trans. Antennas Propag.*, vol. 62, no. 11, pp. 5851–5855, Nov. 2014.
[22] H. Lee, J. Lee, S. Moon, M. Kim, and H. Kim, "Multiband planar monopole antenna using coupling control feed structure for mobile handsets," *Microw. Opt. Technol. Lett.*, vol. 57, no. 4, pp. 823–826, Apr. 2015.
[23] R. Zhang, Y. Liu, H. Kim, and H. Kim, "PIFA using series-resonant feed structure for wide-band operations," *Electron. Lett.*, vol. 51, no. 8, pp. 606–608, Apr. 2015.
[24] H. Shin, J. Jeon, and H. Kim, "Efficiency enhancement of wide-band mobile antenna," *Electron. Lett.*, vol. 52, no. 3, pp. 179–181, Feb. 2016.
[25] H. Shin and H. Kim, "Wideband mobile antenna design using a resonant feeding structure," *J. Electromagn. Eng. Sci.*, vol. 22, no. 3, pp. 252–255, May 2022.
[26] H. Shin and H. Kim, "Enhancing efficiency for wideband antennas by controlling the parasitic resonance of the feed structure," *J. Electromagn. Eng. Sci.*, vol. 22, no. 4, pp. 399–402, Jul. 2022.
[27] X.-Y. Zhang and J.-C. Lee, "A dual-band branch-line coupler with ultra-wideband harmonic suppression," *J. Electromagn. Eng. Sci.*, vol. 23, no. 1, pp. 57–62, Jan. 2023.
[28] J. Jeon, L. Qu, H. Lee, and H. Kim, "Ground radiation antenna for mobile devices using controlled endless metal rim mode," *ETRI J.*, vol. 40, no. 2, pp. 180–187, Apr. 2018.
[29] L. Qu, J. Jeon, D. Park, and H. Kim, "Antenna design based on quasi-degenerate characteristic modes of unbroken metal rim," *IET Microw., Antennas Propag.*, vol. 11, no. 15, pp. 2168–2173, Dec. 2017.
[30] S. Chilukuri and S. Gundappagari, "A wide dual-band metamaterial-loaded antenna for wireless applications," *J. Electromagn. Eng. Sci.*, vol. 20, no. 1, pp. 23–30, Jan. 2020.
[31] D. Wen, Y. Hao, H. Wang, and H. Zhou, "Design of a wideband antenna with stable omnidirectional radiation pattern using the theory of characteristic modes," *IEEE Trans. Antennas Propag.*, vol. 65, no. 5, pp. 2671–2676, May 2017.
[32] Z. Zhang, Y. Cheng, H. Luo, and F. Chen, "Low-profile wideband circular polarization metasurface antenna with characteristic mode analysis and mode suppression," *IEEE Antennas Wireless Propag. Lett.*, vol. 22, pp. 898–902, 2023.
[33] C.-Y.-D. Sim, H.-Y. Liu, and C.-J. Huang, "Wideband MIMO antenna array design for future mobile devices operating in the 5G NR frequency bands n77/n78/n79 and LTE band 46," *IEEE Antennas Wireless Propag. Lett.*, vol. 19, pp. 74–78, 2020.
[34] Y. Li, C.-Y.-D. Sim, Y. Luo, and G. Yang, "High-isolation 3.5 GHz eight-antenna MIMO array using balanced open-slot antenna element for 5G smartphones," *IEEE Trans. Antennas Propag.*, vol. 67, no. 6, pp. 3820–3830, Jun. 2019.
[35] Q. Cai, Y. Li, X. Zhang, and W. Shen, "Wideband MIMO antenna array covering 3.3–7.1 GHz for 5G metal-rimmed smartphone applications," *IEEE Access*, vol. 7, pp. 142070–142084, 2019.
[36] X. Zhang, Y. Li, W. Wang, and W. Shen, "Ultra-wideband 8-port MIMO antenna array for 5G metal-frame smartphones," *IEEE Access*, vol. 7, pp. 72273–72282, 2019.
[37] A. Zhao and Z. Ren, "Wideband MIMO antenna systems based on coupled-loop antenna for 5G N77/N78/N79 applications in mobile terminals," *IEEE Access*, vol. 7, pp. 93761–93771, 2019.
[38] L. Qu, H. D. Kim, and R. Zhang, "High-sensitivity ground radiation antenna system using an adjacent slot for Bluetooth Handsets," *IEEE Tap*, vol. 10, pp. 546–552, 2016.
[39] W. Lee, M. Park, and T. Son, "Hybrid MIMO antenna using interconnection tie for eight-band mobile handsets," *J. Electromagn. Eng. Sci.*, vol. 15, no. 3, pp. 185–193, Jul. 2015.
[40] C. Deng, D. Liu, and X. Lv, "Tightly arranged four-element MIMO antennas for 5G mobile terminals," *IEEE Trans. Antennas Propag.*, vol. 67, no. 10, pp. 6353–6361, Oct. 2019.
[41] H. Huang, Y. Liu, S. Zhang, and S. Gong, "Multiband metamaterial-loaded monopole antenna for WLAN/WiMAX applications," *IEEE Trans. Antennas Propag. Lett.*, vol. 14, no. 2, pp. 662–665, Dec. 2014.
[42] F. M. Tesche, M. Ianoz, and T. Karlsson, *EMC Analysis Methods and Computational Models*. New York, NY, USA: Wiley, 1997.

RUI LI was born in 1998. He received the B.S. degree in communication engineering from Yanbian University, Yanji, China, in 2020. He is currently pursuing the integrated Ph.D. degree with the Department of Electronic Engineering, Hanyang University, Seoul, South Korea. His current research interests include MIMO, multi-wideband, high-efficiency, and mobile miniaturization antennas.

LONGYUE QU (Member, IEEE) received the M.S. and Ph.D. degrees in electromagnetics and microwave engineering from Hanyang University, Seoul, Republic of Korea, in 2015 and 2018, respectively.

He was a Postdoctoral Researcher with Hanyang University, from September 2018 to August 2019, after which he was promoted to an Assistant Research Professor. He was the Co-Founder and the CTO of Hanyang Antenna Design Company Ltd., Shenzhen, China, from 2019 to 2022. Since 2022, he has been with the School of Electronics and Information Engineering, Harbin Institute of Technology, Shenzhen, as an Assistant Professor. He has authored more than 50 articles and more than 30 inventions. His current research interests include antenna theory and designs, metamaterial-based antenna technology, millimeter-wave arrays, and RF circuits.

Dr. Qu is an Editorial Board Member of the *International Journal of Sensors, Wireless Communications and Control*. He was a recipient of Korean Government Scholarship Award and China Scholarship Council. His research was listed in the Top 100 National Research and Development Excellence Award in 2015. He is a reviewer for several international journals and conferences.

SEOK-JU WI received the B.S. degree from Chungnam University, Daejeon, South Korea, in 2020. He is currently pursuing the integrated Ph.D. degree with the Department of Electronic Engineering, Hanyang University, Seoul, South Korea. His research interest includes mobile antenna design based on ground characteristic mode analysis.

HUANXUAN REN was born in Liaoning, China, in 2003. He is currently pursuing the B.S. degree with the Department of Robotization, Shandong University of Science and Technology, Jinan, China, in 2021.

HYEONGDONG KIM was born in Kwangju, Republic of Korea. He received the B.S. and M.S. degrees from Seoul National University, Seoul, Republic of Korea, in 1984 and 1986, respectively, and the Ph.D. degree from the University of Texas in Austin, in 1992. From May 1992 to February 1993, he was a Postdoctoral Fellow with the University of Texas in Austin. In 1993, he was a Professor with the Department of Electrical and Computer Engineering, Hanyang University, Seoul. His current research interests include various antenna theories and designs based on ground characteristic mode analysis, namely, wideband, high-efficiency, circular polarization, MIMO, and high-sensitivity antennas.